$$V_1(x,H) = \frac{\lambda}{2\pi(\epsilon_1+\epsilon_2)} \sum_{n=0}^{\infty} \beta^{n-1} \sum_{m=0}^{\infty} A_{mn} \cdot \left\{ -\beta \log \frac{(x/H)^2 + 4[r(n+1)+m]^2}{(x/H)^2 + 4[r(n+1)+(m-1)]^2} + \log \frac{(x/H)^2 + 4[nr+m]^2}{(x/H)^2 + 4[nr+(m-1)]^2} \right\} \quad (12)$$

where $r = ((E/H) - 1)$. The form of (12) suggests the possibility of a derivation by multiple images. The doubly infinite series in (12) converges rapidly; less than 100 terms are required. For $\epsilon_2 = \epsilon_3$ and $E = H$, (10) reduces to the Green's function for two-layer microstrip [4].

Fig. 4 shows some typical results for a three-layer problem ($\epsilon_1 = 9.6\epsilon_0$, $\epsilon_2 = 2.6\epsilon_0$, $\epsilon_3 = \epsilon_0$). The middle curve ($E/H = 1.206$) represents a three-layer microstrip currently in use. The upper and lower curves correspond to two-region problems and agree precisely with data computed from two-region programs. The middle curve agrees within better than two percent with limited experimental data available. Computation time for a typical curve is about 1 min on the GE-635 computer. Notice that as the thickness of the second dielectric layer increases, the characteristic impedance decreases.

IV. CONCLUSIONS

The multilayer multiconductor microstrip has been treated in general. The three-region microstrip has been analyzed in detail and a general computer program has been prepared. Results appear to be accurate to within a few percent.

REFERENCES

[1] A. Farrar and A. T. Adams, "A potential theory method for covered microstrip," *IEEE Trans. Microwave Theory Tech.* (Short Papers), vol. MTT-21, pp. 494–496, July 1973.
[2] R. F. Harrington, *Field Computation by Moment Methods.* New York: Macmillan, 1968.
[3] A. T. Adams, *Electromagnetics for Engineers.* New York: Ronald, pp. 166–215.
[4] P. Silvester, "TEM wave properties of microstrip transmission lines," *Proc. Inst. Elec. Eng.*, vol. 115, Jan. 1968.
[5] E. Yamashita, "Variational method for the analysis of microstrip-like transmission lines," *IEEE Trans. Microwave Theory Tech.*, vol. MTT-16, pp. 529–535, Aug. 1968.
[6] E. Yamashita and K. Atsuki, "Strip line with rectangular outer conductor and three dielectric layers," *IEEE Trans. Microwave Theory Tech.*, vol. MTT-18, pp. 238–244, May 1970.

A Low-Loss Branching Filter for Broad Widely Spaced Bandwidths

E. A. OHM, MEMBER, IEEE

***Abstract*—A waveguide filter which separates the 4-GHz band from the combined 4-, 6-, and 11-GHz common-carrier bands with a loss of only 0.05 dB is described. The input is limited to a single polarization, but dual polarizations can be accommodated by using two such filters in combination with a polarization coupler. The filter also has low insertion losses at 6 and 11 GHz: 0.1 dB and 0.06 dB, respectively, a good return loss, 32 dB, and a short length, 2½ ft. Additionally, it has high power-handling capability, good isolation properties, and good mode purity.**

INTRODUCTION

Branching networks are widely used in radio systems to connect dual-polarized common-carrier bands to a single antenna [1], but usually these networks are too long and their insertion losses are too large for satellite earth-station use. This has encouraged the development of a new network in which the key parts are a polarization coupler and a branching filter. The mode purity and feasibility of the filter in a dual-polarized feed system have been measured at 4 and 6 GHz, but these characteristics have not been completely evaluated at 11 GHz because only the 4- and 6-GHz bands were of interest in the latest series of measurements. However, the available data indicate that the filter's mode purity is sufficiently good for a dual-polarized 4-, 6-, and 11-GHz system. Such a system would also require a new type of polarization coupler, i.e., one which operates across all three bands. An appropriate coupler has been proposed [2], and deserves further investigation, but a discussion of polarization couplers is beyond the scope of this short paper. Accordingly, the couplers are mentioned only insofar as they are needed to describe the higher order mode measurements of the filter.

Manuscript received February 22, 1974; revised May 13, 1974.
The author is with Bell Laboratories, Holmdel, N. J. 07733.

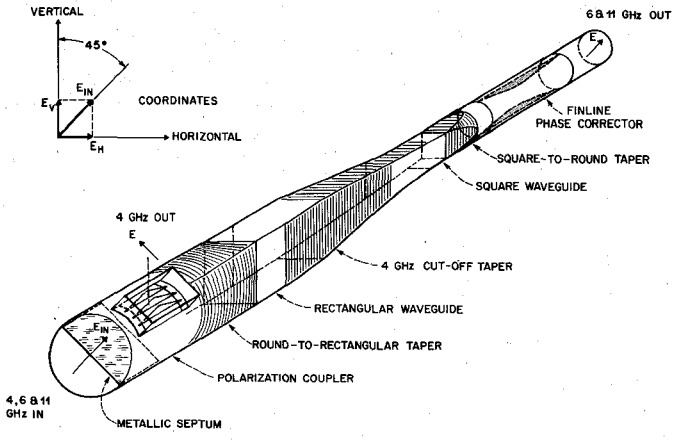

Fig. 1. Principal waveguide surfaces.

PRINCIPLE OF OPERATION

A sketch of the principal waveguide surfaces is shown in Fig. 1. At the round waveguide input on the lower left, which is dominant-mode size at 4 GHz, the dominant-mode signals are inclined 45° with respect to the vertical plane, and are transmitted straight through the polarization coupler. At the coupler output, these are resolved into equal-amplitude vertical and horizontal E-field components, which at 4 GHz are reflected by the cutoff taper, and return to the coupler with a differential phase shift of 180°. To maintain 180° across the 13.6-percent bandwidth, the phase shift is obtained partly from the differential phase shift of the rectangular waveguide, and partly from the longitudinal displacement of the vertical and horizontal walls of the cutoff taper. Adding the E-field components vectorally, the reflected dominant mode is rotated 90°. The rotated polarization is transmitted out of the filter via the side arm of the polarization coupler.

At 6 and 11 GHz (8.4- and 9.3-percent bandwidths), the equal-amplitude vertical and horizontal components are transmitted through the cutoff taper, but with substantially different phase shifts. The difference is reduced to a negligible value by further transmission through the vertically oriented finline phase corrector. As a result, the 6- and 11-GHz components at the main output, on the upper right in Fig. 1, are essentially in phase and add vectorally to yield a polarization which is parallel to that at the input.

The principle of operation is similar to that of a diplexing filter which uses two hybrids and two separate cutoff tapers [3], but here all essential operations are broader band and are performed in a single in-line waveguide.

POLARIZATION COUPLER

For the straight-through path, the coupler in Fig. 1 has a minimum return loss of 47 dB in the 4-GHz band, and 39 dB in the 6- and 11-GHz bands. Around the corner, the minimum return loss is 41 dB in the 4-GHz band. The isolation between the straight-through and around-the-corner polarizations is better than 40 dB.

These results are achieved by proper selection of the height of the triangular plates, and by proper choice of the width of the aperture at the base of the triangles. Additional side-arm tuning is provided by longitudinal positioning of the septum, and by adjustment of small-diameter screws which are in line with and to the right of the septum. The screws (not shown) are in equally inserted pairs, with one on each side of the round waveguide. The coupler operation is similar in principle to single-band models which are described in the literature [4], [5].

The overall filter characteristics are not limited by the polarization coupler, but rather by characteristics of the cutoff taper and the finline phase corrector.

CUTOFF TAPER

Suppose the round waveguide immediately to the right of the polarization coupler is simulated with a square waveguide which has the same cutoff frequency. Suppose also that the square waveguide is simultaneously increased in height and decreased in width with linear tapers to match the cross section of a rectangular waveguide. After a short length of rectangular guide, suppose the height is reduced by a linear taper, and that somewhat further along the width is reduced by another linear taper. The output width is set equal to the output height, and the last two tapers overlap over most of their lengths, i.e., the waveguide height and width are changing simultaneously. A profile of this entire combination of tapers is shown in Fig. 2.

Since the widths and heights taper linearly, the transmission phase shifts are readily calculated. The round-trip phase shifts due to length segments 1 and 4 are determined from [6]

$$\phi = \frac{2\pi l}{a_{\text{in}} - a_{\text{out}}} \left\{ \left[\left(\frac{2a}{\lambda_0} \right)^2 - 1 \right]^{1/2} - \tan^{-1} \left[\left(\frac{2a}{\lambda_0} \right)^2 - 1 \right]^{1/2} \right\}_{a_{\text{out}}}^{a_{\text{in}}} \quad (1)$$

where the a's are transverse dimensions perpendicular to the E-field polarization at the ends of a segment, l is a segment length, and λ_0 is the free-space wavelength. When the transverse dimension is narrowed beyond cutoff for the incident wave, as in segments 3 and 6 at 4 GHz, the lower limit a_{out} becomes $\lambda_0/2$, and (1) reduces to

$$\phi = \frac{2\pi l}{a_{\text{in}} - a_{\text{out}}} \left\{ \left[\left(\frac{2a_{\text{in}}}{\lambda_0} \right)^2 - 1 \right]^{1/2} - \tan^{-1} \left[\left(\frac{2a_{\text{in}}}{\lambda_0} \right)^2 - 1 \right]^{1/2} \right\} + \phi_0 \quad (2)$$

where ϕ_0 allows for phase-shift effects due to fringing fields and partial reflections which occur near the input of each cutoff-taper segment. The round-trip phase shifts due to constant-width segments 2 and 5 are calculated from

$$\phi = \frac{2\pi l}{a} \left[\left(\frac{2a}{\lambda_0} \right)^2 - 1 \right]^{1/2}. \quad (3)$$

Adding the phase shifts of segments 1–3, and separately those of 4–6, the round-trip phase shifts of the horizontal and vertical polarizations are

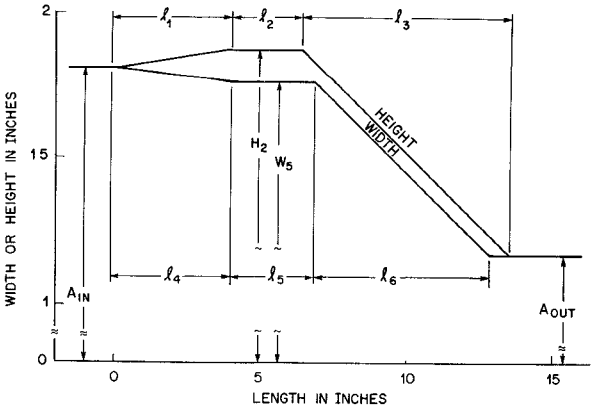

Fig. 2. Dimensional profile of a 4-GHz cutoff taper.

$$\phi_{\text{horizontal}} = \phi_1 + \phi_2 + \phi_3 \quad (4)$$

$$\phi_{\text{vertical}} = \phi_4 + \phi_5 + \phi_6 \quad (5)$$

where ϕ_2 and ϕ_5 are specified by (3), ϕ_3 and ϕ_6 by (2), and ϕ_1 and ϕ_4 by (1). The subscripts 1–3 correspond to taper heights associated with lengths l_1–l_3 in Fig. 2, and similarly the subscripts 4–6 correspond to taper widths associated with lengths l_4–l_6 in Fig. 2.

To insure a good return loss, one of the principal objectives is to achieve a differential phase shift of 180° across the 4-GHz band:

$$\Delta\phi = \phi_{\text{horizontal}} - \phi_{\text{vertical}} = 180°. \quad (6)$$

The difference between the actual and desired phase shift is found by subtracting 180° from both sides of (6):

$$\epsilon = \phi_{\text{horizontal}} - \phi_{\text{vertical}} - 180°. \quad (7)$$

An analysis of (7), based on the dimensional profile of Fig. 2, shows that ϵ is very small when H_2 is somewhat larger than W_5. This is duplicated in practice when the taper-profile dimensions are chosen to minimize known experimental and higher order mode problems. In particular, the input and output widths, A_{in} and A_{out} in Fig. 2, are chosen as large as practical, but small enough to suppress higher order modes at 4 and 6 GHz, respectively. This also allows the side arm of the polarization coupler to be well matched across the 4-GHz band, and the main-output parts to be well matched across the 6- and 11-GHz bands. The slopes of l_3 and l_6 are equal, and to limit higher order mode generation are chosen to limit the angle between each taper wall and the filter's longitudinal axis to less than 3°. A length of $l_6 = 6$ in satisfies the 3° criterion, and furthermore yields a cutoff taper match of better than 40 dB across the 6- and 11-GHz bands. These conditions also minimize changes in ϕ_0 of (2) for the horizontal polarization with respect to ϕ_0 for the vertical polarization. As a result, the corresponding cutoff planes track each other across the 4-GHz band with good precision. This means that ϕ_0 in (2) is reduced as a serious source of error.

The lengths l_1 and l_4 are chosen to be $3\lambda_g/4$ at 3.95 GHz to minimize reflections, and the impedance ratios Z_2/Z_{in} and Z_5/Z_{in} are chosen to yield reflections from slopes l_1 and l_4 which are equal and opposite [7]. Consequently, these reflections do not degrade the performance of the filter at 4 GHz because they add vectorally, are rotated 90°, and are coupled directly into the side arm of the polarization coupler. In Fig. 1, where l_1 and l_4 correspond to the length of the round-to-rectangular taper, the residual reflections in all three bands were virtually eliminated by using polyfoam tuning elements. These did not generate higher order modes at 6 or 11 GHz. With additional effort, they could probably be replaced with conventional tuning elements if it can be shown that the latter do not generate higher order modes.

From the geometry of Fig. 2

$$l_3 = l_6 \frac{H_2 - A_{\text{out}}}{W_5 - A_{\text{out}}} \quad (8)$$

where l_6 and A_{out} have been determined previously. From the Z_2/Z_{in} and Z_5/Z_{in} criteria, W_5 is a unique function of H_2, and therefore for any trial value of H_2 there is a unique value of l_3. The two remaining unknowns in Fig. 2, l_2 and l_5, are calculated by solving two simultaneous equations: (6) at 3.7 GHz and at 4.2 GHz. A series of computations shows that l_2 and l_5 decrease as H_2 is increased. Equation (7) further shows that ϵ is negative, that it is largest in magnitude near midband, and that the peak magnitude increases as H_2 is increased. For the dimensions used in Fig. 2, the peak error in the 4-GHz band is about −4°. This is cut nearly in half by allowing ϵ at the band edges to be equal and opposite to ϵ at the band center. The corresponding theoretical values of l_2 and l_5 are calculated by increasing the right-hand side of (6) from 180° to 182.2°.

With the hardware shown in Fig. 1, it was found experimentally that the optimum values of l_2 and l_5 are shorter than calculated. In particular, when each was shortened 0.125 in, the error ϵ was less than ±2° (with a periodicity of 1½ cycles) across the 4-GHz band.

The principal effect of ϵ is to cause the wave reflected from the cutoff taper to have a cross-polarized component. This is transmitted straight through the polarization coupler rather than transmitted around the corner, and degrades the return loss in accordance with

$$\text{return loss (dB)} = -\text{cross pol (dB)} = -20 \log_{10} [\tan^{-1} \epsilon/2]. \quad (9)$$

For $\epsilon = \pm 2°$, the 4-GHz return loss is 35 dB, which is good enough for most practical purposes.

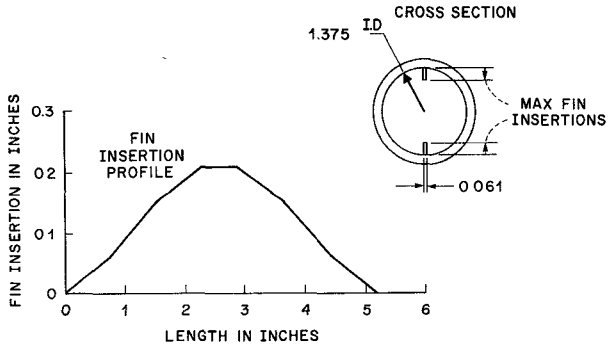

Fig. 3. Finline phase corrector.

FINLINE PHASE CORRECTOR

At the output of the cutoff taper, the differential phase shift, $\Delta\phi = \phi_{\text{horizontal}} - \phi_{\text{vertical}}$, varies smoothly from 57° at the low end of the 6-GHz band to 21° at the high end of the 11-GHz band. In principle, this can be reduced to zero across both bands by using a short finline waveguide with deeply inserted fins. In practice, such a finline [2] is difficult to match, especially across the 6-GHz band. Since a good match is essential, a compromise design was chosen which is shown in Fig. 3. The fin insertion is fairly small, and the length is as short as practical consistent with a good match. Each finline taper is divided into 3 segments of $\lambda_g/4$ each (at 6.14 GHz), where the slopes have a ratio of $1:\sqrt{2}:1$. The length of each fin is chosen such that the residual reflections from one end are phased to cancel those from the other. The resulting return loss is 45 dB across the 6-GHz band, and 38 dB across the 11-GHz band. Experimentally, $\Delta\phi$ at the output of the cutoff taper is reduced by the finline phase corrector to $-3°$ at 5.925 GHz, $+1°$ at 6.425 GHz, and $+2°$ across the 11-GHz band. The residual cross polarization is found by substituting $\Delta\phi$ for ϵ in (9). At the main output port, the cross polarization can be readily absorbed by a transverse resistance card. However, when 6 or 11 GHz are incident at the output port, the cross polarization limits the side-arm isolation to a value predicted by (9). For the worst case, i.e., $\Delta\phi = -3°$, the predicted isolation is 31.6 dB.

EXPERIMENTAL RESULTS

The characteristics of the filter shown in Fig. 1 are summarized in Fig. 4. The insertion loss at 4 and 11 GHz is in good agreement with the theoretical copper loss, but at 6 GHz the peak loss is about 0.06 dB larger than anticipated. This was traced to a mode in the side arm which had an E-field in the unusual direction, i.e., parallel to the wide dimension of the guide. This problem was eliminated in a later model by reducing the size of the side-arm waveguide [8]. The filter was tested with the new coupler at 4 and 6 GHz using swept-frequency techniques, and was found to have return losses and isolations at the same general levels as before. At 6 GHz there was some evidence of higher order TE_{11} and TM_{11} modes excited by the side-arm coupler and trapped between the septum and the 4-GHz cutoff tapers. But the effects of these resonances on the filter transmission characteristics were found to be barely detectable. If better performance should be required, it is of interest to note that the higher order mode excitation can be reduced, at least across the 6-GHz band, by making some minor changes in the new side-arm coupler. In the original coupler, the higher order mode excitation at 11 GHz was found to be less than at 6 GHz. A plausible explanation is that at 11 GHz, the through arm of the side-arm coupler is operated much further from cutoff. The relatively low excitation at 11 GHz is probably also inherent in the new coupler, and accordingly no significant changes are expected from the original 11-GHz characteristics shown in Fig. 4.

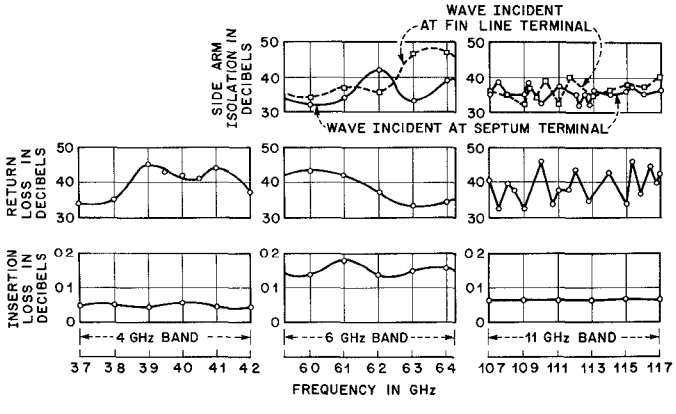

Fig. 4. Filter characteristics.

The feasibility of the filter as part of a dual-polarized feed system was checked at 4 and 6 GHz by connecting two such filters to an earth-station antenna feed via a 4- and 6-GHz polarization coupler. An analysis of the resulting antenna patterns showed that the most troublesome higher order modes were TE_{11} and TM_{11} and that these occurred in the 6-GHz band. However, their levels were down at least 26 dB, with the result that a cross polarization of better than 40 dB could be maintained across one-third the beamwidth of an earth-station antenna operating at 6 GHz.

Although not tested at high power, it seems appropriate to mention that the power-handling capability of the filter is relatively high because the usual buildup in the electric field, due to energy stored in a resonant cavity, has been replaced by a low-Q standing wave caused by reflection from the cutoff taper.

CONCLUSIONS

Broad widely spaced frequency bands can be branched into separate output ports by using a polarization coupler in combination with a waveguide taper and a waveguide finline. The key part for good performance across the low-frequency band is a cutoff taper in which the widths and heights are tapered simultaneously. The taper segments are linear and their dimensions can be readily calculated. For the higher frequency above-cutoff bands, good characteristics can be achieved by adding a finline with a large fin gap. The entire assembly is compact and low loss, and dual polarizations can be accommodated by using two such filters in combination with a polarization coupler.

APPENDIX
TRANSMISSION PHASE SHIFT OF A LINEARLY TAPERED WAVEGUIDE

Consider a waveguide of initial width a_{in} which is linearly tapered with respect to longitudinal distance z. Then the width a is

$$a = a_{\text{in}} - kz. \tag{10}$$

The round-trip phase shift ϕ from the input through a length z is

$$\phi = 2\int_0^z \beta\, dz = 2\int_0^z \frac{2\pi}{\lambda_0}\left[1 - \left(\frac{\lambda_0}{2a}\right)^2\right]^{1/2} dz \tag{11}$$

where β is the dominant-mode phase constant and λ_0 is the free-space wavelength. From (10), $dz = -a/k$ where k is evaluated for an output width a_{out} located at distance $z = l$. Substituting into (11)

$$\phi = \frac{4\pi l}{(a_{\text{out}} - a_{\text{in}})\lambda_0}\int_{a_{\text{in}}}^{a_{\text{out}}}\left[a^2 - \left(\frac{\lambda_0}{2}\right)^2\right]^{1/2}\frac{da}{a}.$$

Integrating

$$\phi = \frac{4\pi l}{(a_{\text{out}} - a_{\text{in}})\lambda_0}\left[\left[a^2 - \left(\frac{\lambda_0}{2}\right)^2\right]^{1/2} - \frac{\lambda_0}{2}\tan^{-1}\left|\frac{[a^2 - (\lambda_0/2)^2]^{1/2}}{(\lambda_0/2)}\right|\right]_{a_{\text{in}}}^{a_{\text{out}}}$$

where the positive value of $[a^2 - (\lambda_0/2)^2]^{1/2}$ is taken, and the $\tan^{-1}$ angle is between 0 and $+\pi/2$. Reversing the limits of integration, and rewriting

$$\phi = \frac{2\pi l}{a_{\text{in}} - a_{\text{out}}}\left\{\left[\left(\frac{2a}{\lambda_0}\right)^2 - 1\right]^{1/2} - \tan^{-1}\left[\left(\frac{2a}{\lambda_0}\right)^2 - 1\right]^{1/2}\right\}_{a_{\text{out}}}^{a_{\text{in}}}$$

which is the result used in (1).

ACKNOWLEDGMENT

The author wishes to thank W. W. Snell for valuable discussions and many timely suggestions.

REFERENCES

[1] E. T. Harkless, "A network for combining radio systems at 4, 6 and 11 kmc," *Bell Syst. Tech. J.*, vol. 38, pp. 1253–1267, Sept. 1959.
[2] S. D. Robertson, "The ultra-bandwidth finline coupler," *Proc. IRE*, vol. 43, pp. 739–741, June 1955.
[3] L. Young and J. Q. Owen, "A high power diplexing filter," *IRE Trans. Microwave Theory Tech.*, vol. MTT-7, pp. 384–387, July 1959.
[4] R. D. Tompkins, "A broad-band dual-mode circular waveguide transducer," *IRE Trans. Microwave Theory Tech.*, vol. MTT-4, pp. 181–183, July 1956.
[5] E. A. Ohm, "A broad-band microwave circulator," *IRE Trans. Microwave Theory Tech. (Special Issue: National Symposium on Microwave Techniques)*, vol. MTT-4, pp. 210–217, Oct. 1956.
[6] E. T. Harkless, "Transmission phase shift of a linearly tapered waveguide," Appendix.
[7] G. A. Southworth, *Principles and Applications of Waveguide Transmission*, 5th printing. Princeton, N. J.: Van Nostrand, 1961, eq. (5.2-6) and (3.5-3).
[8] J. J. Erlinger, Rantec, Calabasas, Calif., private communication.

Pump Noise Transfer in Parametric Amplifiers

W. A. PORTER, MEMBER, IEEE, D. I. BREITZER, MEMBER, IEEE, AND B. SMILOWITZ

***Abstract*—Pump noise transfer in paramps is related to the sensitivity of amplifier gain to AM and FM pump modulation. Measurements performed on an *S*-band paramp with an 18.4-GHz pump are described. The significance of the results is made explicit by using them to calculate the increase in amplifier noise temperature associated with an IMPATT oscillator pump.**

I. INTRODUCTION

The noise figure of parametric amplifiers has been observed [1]–[3] to increase as a result of pump noise, when a strong signal is present in the passband. Of the various oscillators available for pump sources, the IMPATT oscillator has the greatest noise content and, thus, is more prone to produce this effect. This note presents data on pump noise transfer and an estimate of the effect produced by IMPATT oscillators. The basic premise in this work is that pump noise causes the amplifier gain to vary, and that sinusoidal pump modulation can be used to obtain quantitative results about this phenomenon.

II. ANALYSIS

Modulation of the pump amplitude and frequency, E_p and f_p, produces variations in the amplitude and phase, $G^{1/2}$ and ϕ, of the voltage reflection coefficient, and this, in turn, modulates the output of any signal E_s applied to the amplifier. For harmonic pump modulation at frequency f_m, the variation of the reflection coefficient and output voltage can be formally expressed as follows:

$$\delta G^{1/2} = \left(\frac{\partial G^{1/2}}{\partial E_p}\right)\delta E_p + \left(\frac{\partial G^{1/2}}{\partial f_p}\right)\delta f_p = \left(\frac{\partial G^{1/2}}{\partial E_p}\right) 2\Delta E_p \cos\,(2\pi f_m t + \theta_E) + \left(\frac{\partial G^{1/2}}{\partial f_p}\right) 2\Delta f_p \cos\,(2\pi f_m t + \theta_f)$$

$$\delta\phi = \left(\frac{\partial \phi}{\partial E_p}\right)\delta E_p + \left(\frac{\partial \phi}{\partial f_p}\right)\delta f_p = \left(\frac{\partial \phi}{\partial E_p}\right) 2\Delta E_p \cos\,(2\pi f_m t + \theta_E) + \left(\frac{\partial \phi}{\partial f_p}\right) 2\Delta f_p \cos\,(2\pi f_m t + \theta_f)$$

$$\delta E_{so} = (\delta G^{1/2} + jG^{1/2}\delta\phi)\,\exp\,(j\phi)E_{si}$$

where ΔE_p and Δf_p are, respectively, the voltage and frequency amplitudes of the AM and FM sidebands, and θ_E and θ_f are arbitrary phase constants.

The amplitude and frequency modulation of the pump are now considered separately. For pure AM on the pump ($\Delta f_p = 0$), the power $P_{so}(\mathrm{AM})$ in each of the output signal sidebands is given by

$$P_{so}(\mathrm{AM}) = \left\{\left(\frac{\partial G^{1/2}}{\partial E_p}\right)^2 + G\left(\frac{\partial \phi}{\partial E_p}\right)^2\right\}(\Delta E_p)^2 P_{si} = K(\mathrm{AM})\left(\frac{P_p(\mathrm{AM})}{P_p}\right)(GP_{si}) \quad (1)$$

where P_{si} is the input signal power, $[P_p(\mathrm{AM})/P_p]$ is the pump sideband to carrier ratio, and $K(\mathrm{AM})$ is the AM sensitivity coefficient defined by

$$K(\mathrm{AM}) \equiv \left(\frac{P_p}{G}\frac{\partial G}{\partial P_p}\right)^2 + \left(2P_p\frac{\partial \phi}{\partial P_p}\right)^2.$$

For pure FM on the pump ($\Delta E_p = 0$), the result is

$$P_{so}(\mathrm{FM}) = \left\{\left(\frac{\partial G^{1/2}}{\partial f_p}\right)^2 + G\left(\frac{\partial \phi}{\partial f_p}\right)^2\right\}(\Delta f_p)^2 P_{si} = K(\mathrm{FM})\left(\frac{f_m}{f_p}\right)^2\left(\frac{P_p(\mathrm{FM})}{P_p}\right)(GP_{si}) \quad (2)$$

where the sideband to carrier ratio is related to the frequency deviation by

$$\frac{P_p(\mathrm{FM})}{P_p} = \left(\frac{\Delta f_p}{f_m}\right)^2$$

and the FM sensitivity coefficient is defined by

$$K(\mathrm{FM}) = \left(\frac{f_p}{2G}\frac{\partial G}{\partial f_p}\right)^2 + \left(f_p\frac{\partial \phi}{\partial f_p}\right)^2.$$

Equations (1) and (2) provide the analytic framework for the measurements described in the following sections. The general defining relations for $K(\mathrm{AM})$ and $K(\mathrm{FM})$ have been applied to a specific model for a parametric amplifier. The salient result of this work is that the sensitivity parameters are proportional to the amplifier gain. A detailed description of this work will be presented in a forthcoming paper on the theory of pump noise transfer in parametric amplifiers.

III. MEASUREMENTS

Measurements were performed on an AIL 381088 parametric amplifier which had a double-tuned signal circuit centered at 2.24 GHz and an 18.4-GHz Gunn oscillator pump source. The gain response curve for this amplifier is shown in Fig. 1. The measurements took the following form: the pump was sinusoidally modulated, a strong input signal was applied to the amplifier, and the modulation sidebands on the amplifier output signal were monitored. The parameters that were independently varied included the input signal frequency, input signal power, pump modulation frequency, and pump modulation ratios.

The measured data had the general behavior described in (1) and (2)—that is, the output signal sidebands increased linearly with the pump modulation ratio and the input signal power. In addition, the AM results were independent of the modulating frequency, while the FM data showed an average increment of 6 dB/octave, as expected. Equations (1) and (2) were used to convert the raw data for the various experimental conditions into values of the sensitivity co-

Manuscript received February 25, 1974; revised June 10, 1974.
The authors are with AIL, Division of Cutler-Hammer, Deer Park, Long Island, N. Y. 11729.